Effective Way of Modeling Chemical Catalysis: Empirical Valence Bond Picture of Role of Solvent and Catalyst in Alkylation Reactions

JORDI VILLÀ,[1,2,3] JÖRG BENTZIEN,[2,4] ÀNGELS GONZÁLEZ-LAFONT,[1] JOSÉ M. LLUCH,[1] JUAN BERTRAN,[1] ARIEH WARSHEL[2]

[1]*Departament de Química, Universitat Autònoma de Barcelona, 08193 Bellaterra, Barcelona, Spain*
[2]*Department of Chemistry, University of Southern California, Los Angeles, California*
[3]*Grup de Recerca en Informàtica Mèdica, Institut Municipal d'Investigació Mèdica, Barcelona, Spain*
[4]*Xencor, Pasadena, California*

Received 17 September 1999; accepted 12 January 2000

ABSTRACT: A general methodology for the study of chemical catalysis is presented and demonstrated in a study of Friedel–Crafts-type alkylation reactions that are constrained to collinear configurations. *Ab initio* potential energy surfaces in solution and relevant experimental results are used to calibrate general empirical valence bond (EVB) potential surfaces for studies of such reactions. The EVB surfaces allow one to interpolate the *ab initio* results to studies of the effect of different solvents, substituents, and catalysts on the alkylation reactions. This implicit approach introduces such effects by shifting the diagonal energies of the corresponding resonance structures. Such an EVB/shift approach appears valuable for assessing the effects of different catalysts and solvents on complex chemical reactions. © 2000 John Wiley & Sons, Inc. J Comput Chem 21: 607–625, 2000

Keywords: empirical valence bond (EVB); Langevin dipoles (LD); alkylation reactions; chemical catalysis; complex reactions

Correspondence to: J. M. Lluch; e-mail: lluch@klingon.uab.es
Contract/grant sponsor: EMBO; contract/grant number: ALTF 509-1998
Contract/grant sponsor: NIH; contract/grant number: GM24492

Introduction

Studying chemical catalysis by computer modeling approaches can, at least in principle, increase the insight gained from experimental studies and help to optimize the catalyst used. This is, of course, a major challenge when applied to *real* chemical systems, where many factors can be involved. Let us consider, for example, a Friedel–Crafts-type alkylation reaction. Friedel and Crafts discovered the aluminum chloride-catalyzed alkylation of benzene with alkyl halides in 1877.[1] In particular, they obtained toluene by passing a current of methyl chloride into benzene-containing aluminum chloride and heating gently.[1] Nowadays, however, there are not one but many reactions bearing the general name of "Friedel–Crafts."[2] Testing of various alkyl halides has shown that the alkyl fluorides are the most reactive, with boron trifluoride a very suitable catalyst for this alkylation reaction.[2–4] Alkylation generally occurs most readily with tertiary halides and benzyl halides, less readily with secondary halides, and least readily with primary halides. In the series of primary halides, methyl halides are the least reactive.[4] A more inert halide requires a more powerful catalyst.[4] The course of the Friedel–Crafts reaction is greatly affected not only by the catalyst but also by the solvent.[5] Furthermore, in discussing Friedel–Crafts alkylation reactions, it is difficult to distinguish between solvent and catalytic effects and thus the two are best considered together.[4] Nonpolar as well as polar solvents,[2,6] like nitromethane, nitrobenzene, acetonitrile,[2,5,6] and, in some special cases, water, have been used.[7]

Such a complex process can be represented schematically by a general reaction:

$$cat + R_S X + R_A H + solv \rightarrow cat\text{-}X^- + R_S R_A + solv\text{-}H^+$$

where *cat* stands for the catalyst, R_S is the substituent of the alkylation agent, R_A is the acceptor, *solv* is the solvent, and X is the halide. Despite the fact that Friedel–Crafts reactions have been a very powerful synthetic method, the mechanism of this type of reactions is not fully established. It has been shown that a substantial number of complexes between the *n*-donor alkyl halide and the Lewis acid can be isolated as stable chemical entities.[3,8] Depending on the catalyst, the solvent, the reaction conditions, and the alkyl halide the formation of a polarized donor–acceptor complex or real carbocations (either as an ion pair or a free entity) may take place.[9] For these two possibilities, Friedel–Crafts alkylation can occur either via a displacement mechanism involving a nucleophilic attack on the alkyl halide–Lewis acid halide complex[10] or a direct alkylation by the carbonium ion.[11] The involvement of different factors and the feasibility of different mechanisms makes the theoretical analysis of Friedel–Crafts-type reactions a major challenge for computational chemists. Full quantum determination of the potential surfaces of such reactions in different environments and with different catalysts represents an enormous effort. Thus, it is important to devise alternative approaches that would allow one to analyze the role of different factors in such reactions.

The valence bond (VB) method has been used successfully to analyze the gas-phase potential energy surfaces in both qualitative[12] and quantitative[13] ways. The physics of the method is particularly suitable for describing bond-breaking and bond-making processes and in describing the relationship between related reactions.[14] This feature was exploited by Warshel and coworkers[14] who realized that the VB picture can provide what is probably the easiest way for obtaining a consistent description of environmental effects on chemical reactions. Such a description was obtained with the so-called empirical valence bond (EVB) method. This method uses VB-like diabatic states to represent the diagonal energies and forces these states to provide the exact energy of the system at its asymptotic region (i.e., the fragments at infinite separation). The diabatic states are then mixed by off-diagonal matrix elements to provide the actual ground state of the system. The main difference between the EVB model and the VB model is the idea that external effects, such as solvent effects, can be described quantitatively and consistently by considering their effect on each diabatic state (before mixing these states) and by forcing these diabatic states to reproduce the corresponding experimental (or accurate theoretical) results at the asymptotic region. The effects of the external factors on the system at the reaction region is obtained by mixing the diabatic states using the proper off-diagonal elements, which are calibrated using the properties of a reference system (e.g., the experimental and theoretical properties of the gas-phase system). The realization that the seemingly simple EVB method is in fact a quantitative and consistent quantum-mechanical/molecular-mechanics (QM/MM) method, which is particularly effective

in studies of environmental effects, led other workers to adopt this method[15] (see also ref. 16).

The incorporation of the effect of different solvents in the EVB method involves the shifts of the energies of the diabatic states, in their asymptotic regions, by the corresponding solvation energies. The polarization of the system at the reaction region is then obtained by evaluating the solvation of the diabatic states whose charges are fixed (because they represent pure states) and self-consistent calculations of the ground-state charges, the corresponding solvent polarization, and the new solvation of the diabatic states. With this procedure in mind, it is reasonable to describe substituent effects and, more importantly, the effect of different catalysts by the proper shifts of the energies of the diabatic states. For example, one can force the asymptotic energies of the diabatic states to reproduce the change in effective ionization energies and electron affinities due to the presence of the given catalyst. The change of the potential surfaces at the reaction region is then evaluated by mixing the shifted diabatic states with unchanged off-diagonal terms. The implementation of this "energy-shift" idea in studies of chemical catalysis is the primary focus of the present work.

The present study involves a simplified version of the EVB model where the solvent is represented by the Langevin dipoles (LD) model. This approach provides a self-consistent solute–solvent coupling, but does not give a rigorous description of nonequilibrium solvation effects. A much more rigorous treatment can be obtained by using the free energy perturbation (FEP)/umbrella sampling treatment of the all-atom EVB version.[14d] However, the simplified LD model allows us to illustrate the main points and also provides a very efficient way of calibrating EVB surfaces using *ab initio* results. Such calibrated surfaces can be used conveniently in the refinement of all-atom EVB surfaces.

This work examines our energy shift approach using simplified Friedel–Crafts-type alkylation reactions, where the reaction pathways and the potential surface are restricted to the collinear subspace of the available configurations. This is done as an illustration of the potential of the EVB approach as a general way of describing and predicting catalytic effects and not as an attempt to find the transition state of real alkylation reactions. In doing so, we start by evaluating the potential energy surface along a restricted reaction pathway for the methylation of methane by methylfluoride in water with *ab initio* calculations that involve the use of the LD solvent model.[14] This initial model reaction does not occur in reality, but it will allow us to show the potential of our approach for such complex reactions. The *ab initio* surface and relevant experimental information are used to calibrate an EVB surface. The EVB description is then extended to include the effect of different catalysts and solvents on the calibrated surface.

Methodology

The EVB model has been described in full detail elsewhere,[14] and has been discussed extensively in the last 20 years in many works. Here, only some basic aspects will be recalled. As mentioned earlier, the VB framework easily lends itself to parameterization, whereby the number of resonance structures (RS) can be reduced considerably while still retaining an accurate description of the potential energy surface. Thus, with a fairly small number of VB functions, it is possible to fit a VB model so that it can, for example, reproduce a given *ab initio* surface obtained by molecular orbital (MO) methods or available gas-phase experimental data for the relevant reaction. Moreover, it is possible to use solution experiments to calibrate the VB Hamiltonian, thereby avoiding some of the problems associated with incorporating surrounding medium effects on a vacuum potential. The analytical form of these VB functions can be rather simple by making use of molecular mechanics (MM)-type analytical potentials (see later). A calibration procedure is used to assure that the surface provides the correct asymptotic behavior.

In the present work, we start by calibrating the potential energy surface for the collinear pathways of the Friedel–Crafts-type reaction:

$$CH_3F + CH_4 + H_2O \rightarrow F^- + CH_3CH_3 + H_3O^+ \quad (1)$$

This reference reaction *does not occur in reality* and cannot be catalyzed in water. However, studying this reaction allows us to show the potentiality of the methodology and to demonstrate general aspects of solvent effects.

Before considering the EVB representation of this surface, we explored its feature by first performing gas-phase *ab initio* calculations and then *ab initio* calculations of the reaction in solution. This study was restricted to the linear arrangement shown in Figure 1. The introduction of such a constraint means that we do not explore the reaction path that leads to the three-center bond transition state of the form shown in the diagram:

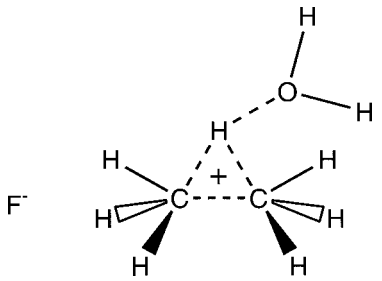

Transition states of this type are quite possible,[9] but our preliminary study indicated that in solution the energies of the three-center bond transition state and the collinear transition state are similar. The results of this *ab initio* study are not given here due to difficulties in locating the exact transition state in solution and also because the focus of the present study is the illustration of our approach rather than the challenging task of determining the potential surfaces of Friedel–Crafts reactions in solution. The gas-phase calculations were performed at the Hartree–Fock level with the 6-31G(d) basis set on a relaxed grid. The system was constrained to be linear, as discussed earlier, and a grid was constructed by varying the $R_{C—F}$ and the $R_{C—C}$ distances using increments of 0.2 Å, within the intervals 1.37–7.37 Å and 1.08–4.08 Å, respectively. The other degrees of freedom were allowed to relax, but forcing the system to be linear. In this way, a total of 496 relaxed grid points were calculated. The gas-phase calculations were performed with the GAUSSIAN-94 program.[19] The solution calculations were performed by using the iterative Langevin dipoles (ILD) model implemented in the program CHEMSOL[20, 21] (version 1.12). The solute charge distribution in the LD calculations was approximated by atom-centered point charges and, in this case, we approximated solute polarization by the solvent using *ab initio* molecular electrostatic potential (MEP) charges of the hydrated solutes that were obtained from polarizable continuum method (PCM) calculations.[22] Hartree–Fock 6-31G(d) wave functions and default Pauling (Merz–Kollman) van der Waals radii, scaled by 1.2, were used for the PCM calculations.[20, 21]

In Tables I to VII relevant information for the calibration of the EVB potential surface is given. With sufficient information about the energetics of the reaction we can turn to obtaining and calibrating the corresponding EVB potential surface. This was done by considering the following three RSs, which can also be seen in Figure 2:

$$\begin{aligned} &\text{(I)} && CH_3F + CH_4 + H_2O \\ &\text{(II)} && F^- + CH_3^+ + CH_4 + H_2O \\ &\text{(III)} && F^- + CH_3{—}CH_3 + H_3O^+ \end{aligned} \qquad (2)$$

The analytical expression of the diagonal gas-phase elements of the EVB Hamiltonian uses MM potentials, adopting a Morse potential function to introduce the anharmonicity for the broken and formed bonds and taking *ab initio* charges for the different species. The expressions for the gas-phase

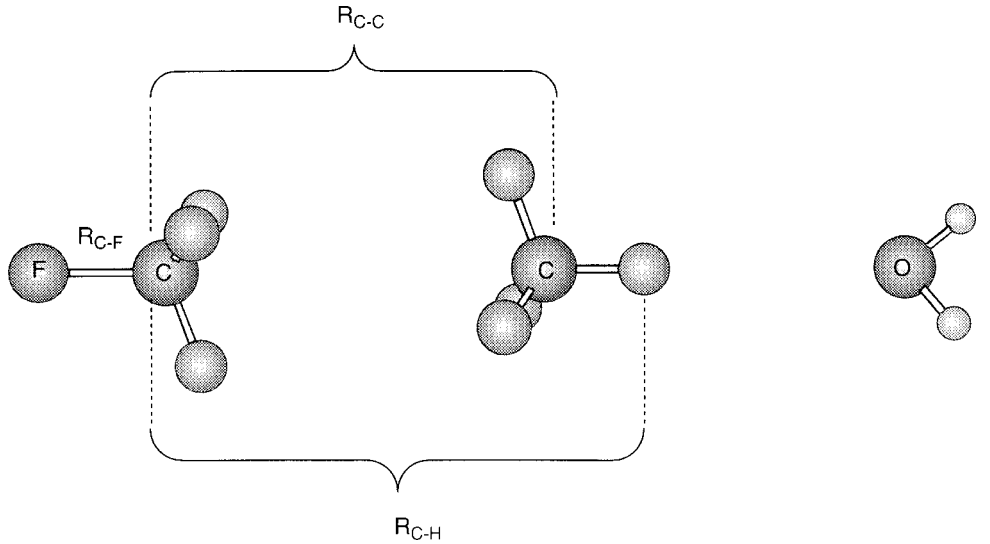

FIGURE 1. A schematic representation of the model reaction and the distances referred in the text.

TABLE I.
Thermodynamic Data for Alkylfluorides (in kcal/mol).

Alkylfluoride	ΔG_f^{gas}	ΔG_{solv}^{wat}	Dissociation Energy
Methylfluoride	−51.6[a]	1.7[b]	108.0[c]
Ethylfluoride	−50.4[a]	−1.5[d]	108.0[e]
i-Propylfluoride	−48.8[a]	−2.1[d]	105.0[e]
t-Butylfluoride	−17.5[f]	−1.5[d]	100.0[g]

[a] Ref. 37.
[b] Ref. 38.
[c] Ref. 39.
[d] LRA.[30]
[e] Ref. 40.
[f] Ref. 41.
[g] Assumed value.

diagonal terms are:

$$\varepsilon_i = H_{il}^0 = \sum_j \Delta M_j^{(i)}\left(b_j^{(i)}\right) + \sum_l \gamma_l^{(i)} k_l^{(i)}\left(\theta_l^{(i)} - \theta_{0,l}^{(i)}\right)^2 + V_{nb}^{(i)} + \alpha^{(i)} \quad (3)$$

where $\Delta M_j^{(i)}$ denotes the Morse potential relative to its minimum value for the *j*th bond in the *i*th VB structure. The second and third terms, respectively, denote the bond angle bending contribution and the nonbonded electrostatic and van der Waals interactions between the reacting groups. The factor, $\gamma_l^{(i)}$, in the second term is a coupling between bonds that are being broken or formed and those angles that depend on these bonds. The parameters used here for the different terms in eq. (3), with the exception of the $\alpha^{(i)}$ terms, have been taken from the general purpose program ENZYMIX.[14g] In implementing the EVB approach, it is essential to have a single reference for all the diagonal energies. This is accomplished by adding a term, $\alpha^{(i)}$, to each diagonal element. The $\alpha^{(i)}$ terms must be calibrated

TABLE II.
Thermodynamic Data for Carbocations (in kcal/mol).

Carbocation	ΔG_{solv}^{wat}	Ionization Potential
Methylcation	−90.0[a]	227.0[b]
Ethylcation	−66.3[c]	193.6[b]
i-Propylcation	−60.9[c]	172.8[b]
t-Butylcation	−55.3[c]	171.0[b]

[a] Ref. 14a.
[b] Ref. 39.
[c] LRA.[30]

TABLE III.
Thermodynamic Data for Products (in kcal/mol).

Product	ΔH_f^{gas}	ΔG_f^{gas}	ΔG_{solv}^{wat}
Ethane	−20.1[a]	−7.9[a]	4.0[b]
Propane	−25.2[a]	−5.6[c]	−2.0[d]
i-Butane	−32.3[a]	−5.0[c]	−2.3[d]
Neopentane	−40.4[a]	−4.1[e]	2.7[d]
Toluene	12.1[a]	29.2[f]	1.0[b]
Ethylbenzene	7.2[a]	31.2[f]	−0.9[d]
Cumene	1.0[a]	32.7[f]	−0.3[d]
t-Butylbenzene	5.4[a]	34.9[f]	0.0[g]

[a] Ref. 39.
[b] Ref. 38.
[c] Ref. 37.
[d] Ref. 42.
[e] Ref. 43.
[f] Ref. 44.
[g] Assumed value.

to reproduce the difference between the asymptotic energies of different RSs; that is, the energies evaluated at the configuration where the fragments of each RS are at infinite separation. In the present study, the agreement between *ab initio* calculations and experimental heats of formation of the different species is good enough for obtaining a reliable potential energy surface. Thus, the $\alpha^{(i)}$ values have been modified to finally reproduce the experimental results in solution. This has been done by taking from the literature experimental data and building the thermodynamic cycles corresponding to each process in solution (I → II and II → III). Then, the $\alpha^{(i)}$ values are modified for our calculations to reproduce those thermodynamic cycles in solution (see Schemes 1–6 for each particular reaction). Given the lack of kinetic experimental results in the hypothetical model reaction, the off-diagonal gas-phase matrix elements have been fitted to reproduce *ab initio* results. For these terms, the following simple

TABLE IV.
Thermodynamic Data for Acceptors (in kcal/mol).

Acceptor	ΔG_f^{gas}	ΔG_{solv}^{wat}
Methane	−12.1[a]	4.1[b]
Benzene	31.0[c]	1.0[b]

[a] Ref. 39.
[b] Ref. 38.
[c] Ref. 44.

TABLE V.
Thermodynamic Data for Solvents (in kcal/mol).

Solvent	ΔG^{wat}_{solv}	H^+ Affinity	$\Delta G^{wat}_{solv}(H^+)$[h]	Dielectric Constant
Water	−4.4[a]	166.5[c]	−102.0[b]	80.0
Nitromethane	−1.8[a]	180.0[d]	−60.0[b]	34.3[f]
HF	−4.8[b]	123.7[e]	−98.7[b]	84.0[g]

[a] Ref. 38.
[b] LD.[20, 21]
[c] Ref. 45.
[d] Ref. 46.
[e] Obtained from *ab initio* 6-311G(d,p) level for the $X—H^+ \rightarrow X + H^+$ reactions.
[f] Ref. 47.
[g] Ref. 39.
[h] Refers to the free energy of solvation in water of the protonated species.

function has been adopted:[14]

$$H^0_{ij} = A_{ij} \exp(-\mu_{ij} r) \tag{4}$$

For H^0_{12}, r is the $R_{F—C}$ distance and for H^0_{23} it corresponds to $R_{C—H}$, the distance between C and the leaving H, where, in both cases, C stands for the carbon atom initially bonded to the fluorine atom, as shown in Figure 1 (note that, for clarity, the arabic 1, 2, and 3 subscripts stand for the corresponding aforementioned diabatic states marked with roman numbers). H^0_{13} has been taken to be equal to zero. A_{ij} and μ_{ij} for H^0_{12} and H^0_{23} have been chosen to fit *ab initio* results at several points on the *ab initio* surface in solution.

TABLE VI.
Thermodynamic Data for Catalysts (in kcal/mol).

Catalyst	ΔG^{gas}_f	ΔG^{wat}_{solv}	F^- affinity
HF		−4.8[b]	−51.5[e]
HF_2^-		−84.8[b]	
BF_3	−267.8[a]	−0.8[c]	−92.0[f]
BF_4^-		−51.8[c]	
SbF_5		0.0[d]	−122.0[g]
SbF_6^-		−43.9[c]	

[a] Ref. 39.
[b] LD.[20, 21]
[c] LRA.[30]
[d] Assumed value.
[e] Obtained from *ab initio* 6-311G(d,p) calculations.
[f] Ref. 48.
[g] Obtained from *ab initio* HF calculations using the 6-311 G(d,p) basis set for F and the pseudopotential of Hay and Wadt[29] with a standard valence double-ζ LANL2DZ contraction for Sb.

The effect of the solvent on our reaction Hamiltonian is obtained in the rigorous all-atom solvent model[14a] (which is not used here) by adding the corresponding energy terms to the diagonal gas-phase matrix elements, H^0_{ii}, leaving unmodified the off-diagonal terms:

$$\begin{aligned} H_{ii} &= H^0_{ii} + U^{(i)}_{Ss} \\ H_{ij} &= H^0_{ij} \end{aligned} \tag{5}$$

where S and s represent the solute and solvent, respectively, and U_{Ss} is the interaction between the solute and solvent atoms. The U_{Ss} terms are calculated for the given configuration of the solvent atoms and involve the interaction between the solvent and the fixed charges of each diabatic state. The actual ground state charges, which are of course not fixed, are obtained by diagonalizing the EVB Hamiltonian:

$$\mathbf{H}\mathbf{C}_g = E_g \mathbf{C}_g \tag{6}$$

This diagonalization also gives the ground-state energy, E_g, for the given solvent orientation. The assumption of leaving the off-diagonal terms unmodified is as least as realistic as the linear free energy relationships or Marcus relationships used by the

TABLE VII.
Atomic Thermodynamic Data (in kcal/mol).

Atom	ΔG^{gas}_f	$\Delta G^{wat}_{solv}(X^-)$	IP	EA
Hydrogen	48.6[a]		313.0[a]	
Fluorine	14.8[a]	−105.0[b]		78.0[b]

[a] Ref. 39.
[b] Ref. 38.

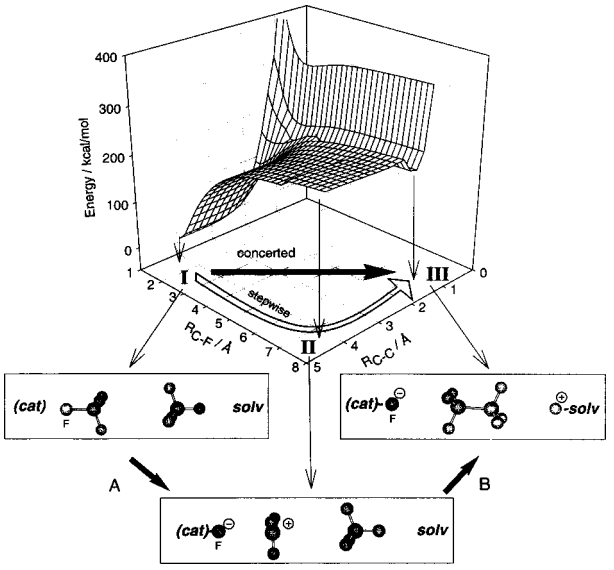

FIGURE 2. *Ab initio* 6-31G(d) potential energy surface in the gas phase for the hypothetical reference reaction $FCH_3 + CH_4 + H_2O \rightarrow F^- + CH_3CH_3 + H_3O^+$. The white arrow indicates the stepwise mechanism studied in this work, with the three most significant RSs indicated schematically. *cat* stands for the molecule that stabilizes the fluoride anion (namely HF, BF_3, and SbF_5). Such a molecule is not considered in the model reaction but introduced in the following reactions. *solv* stands for the different solvents used. As discussed in the text, the solvent participates in two complementary ways: (1) taking part in the chemistry by accepting the proton originated in step B; and (2) by providing the solution environment. This solvent is taken to be water in the *ab initio* calculations of the reference reaction.

experimental community for half a century. This assumption has been justified because the changes in the off-diagonal terms are usually of second order in the expansion of the overlap matrix,[14b] and it is also the subject of current studies.[17] Furthermore, this assumption has been verified in studies of hydride transfer reactions.[23] The use of fixed charges in each diabatic state is the essence of using VB-type treatment where one mixes pure states. In principle, one can include induced dipoles in each diabatic state to represent the mixing of VB structures that are not included explicitly, and such treatment has been used in some studies.[14b] However, it appears that one can obtain reliable results without considering the polarization of the diabatic states. This is particularly true for reactions in solution. At any rate, the effect of the solvent on the ground state of the system is obtained by considering its effect on each diabatic state and then using eq. (6) to obtain the solute charges. The solvent polarization is then obtained rigorously by a molecular dynamics (MD)-FEP/umbrella sampling procedure that properly reflects the solute–solvent interaction and the so-called nonequilibrium solvation effects.[14d] In the present work, however, we represent the solvent using a simplified LD model. In this model, we use the following iterative expression:

$$H_{ii}^{(n+1)} = H_{ii}^{0} + \sum_k q_k^{(i)} U_k^{(n)} - \frac{1}{2}\sum_k Q_k^{(n)} U_k^{(n)} \quad (7)$$

where $U_k^{(n)}$ is the potential at the kth solute atom from the solvent dipoles in their nth iteration; $q_k^{(i)}$ are the atomic charges of the ith RS obtained from PCM calculations as explained earlier and Q_k are the ground-state charges obtained by solving the equation:

$$Q_k^{(n)} = \sum_i (C_{gi}^{(n)})^2 q_k^{(i)} \quad (8)$$

where $C_{gi}^{(n)}$ is the ith component of the ground-state eigenvector of the secular eq. (6). The term

$$-\frac{1}{2}\sum_k Q_k^{(n)} U_k^{(n)}$$

reflects the energy invested in polarizing the solvent by the ground-state charges. Both ILD (where the dipoles "see" each other in the calculation) and noniterative Langevin dipoles (NLD; where the solvent dipoles only "see" the effect of the charges on the solute), have been employed in solving the above equations (see ref. 14a for more details), but only the ILD gave reliable results.

Although our LD approach in this simple implementation does not capture nonequilibrium solvation effects, as the solvent is equilibrated with the solute charges (see discussion in ref. 24), as stated earlier, such effects can be examined by our all-atom free energy perturbation/umbrella sampling approach. Note that, in this respect, many of the current QM/MM approaches do not capture nonequilibrium solvation effects (see ref. 24) and that alternative approaches that use gas-phase charges and reaction coordinates (e.g., ref. 25) do not involve consistent solute–solvent coupling and do not reflect properly the entropy effects of the solute motion (this effect is captured by the all-atom EVB models). At any rate, the present EVB/LD approach is expected to provide simple and reasonably accurate insight about the role of the solvent and the catalyst. EVB/LD calculations have been carried out by using the program SIMPLEVB,[26] which merges the LD treatment of eqs. (7) and (8) implemented in the program CHEMSOL[20, 21] with the ENZYMIX force

field[14a] for the diagonal terms in gas phase [eqs. (3) and (5)].

The EVB surfaces have been parameterized by forcing them to produce the *ab initio* solvation energy surface as well as the relevant experimental values. A first fitting was carried out by means of a genetic algorithm (GA),[27a] as implemented in the Carroll's genetic algorithm driver,[27b] allowing the variation of the $\alpha^{(i)}$ gas-phase values and of the resonance integral parameters, A_{ij} and μ_{ij}, in order to match the CHEMSOL//6-31G(d) values at selected points on the surface. This driver was used successfully by some of us in previous fittings of potential energy surfaces to experimental rate constants.[28] The fitness function to be maximized by the GA has deliberately been chosen to be extremely simple:

$$\text{fitness} = -\sum_{i=1}^{N} \left| E^i_{g,\text{EVB}} - (E + \Delta G_{solv})^i_{ab\ initio} \right| \qquad (9)$$

where N was taken as 5, corresponding to the three minimum energy values for the RSs and the two points on the *ab initio* surface connecting them. The size of the population was taken as 10 individuals per generation with a total of 100 generations, a probability for mutation of 0.1, a crossover probability of 0.5, and a number of children per couple of parents of 1.

The data in Tables I–VII were collected from the literature when available and were used to perform a further correction of the parameters. The fluoride affinity for SbF_5 was estimated by *ab initio* calculations at the Hartree–Fock level with the 6-31G(d) basis set and the pseudopotential of Hay and Wadt[29] with a standard valence double-ζ LANL2DZ contraction for Sb. Some of the free energies of solvation were estimated by using the linear-response approximation (LRA)[30] as implemented in ENZYMIX. In other cases, CHEMSOL itself was used.

Results

The entire reference system depicted in eq. (1) can be divided into three subsystems. These are the substituent of the alkylation agent, CH_3^+; the acceptor, CH_4; and the solvent, H_2O. Note the double role of the solvent as the proton acceptor and the surrounding environment. A fourth subsystem, not represented in eq. (1), is the catalyst. The strategy adopted in this work is to study initially the hypothetical reaction in eq. (1) using EVB methodology. Then, examine more general processes by properly shifting the energies of the EVB diabatic states, resulting in changes of the different subsystems as shown in eq. (1). So, we first present the results of the model reaction obtained by the EVB method. Then, the changes in activation free energy obtained by the shifts in EVB surface, when one takes into account several catalysts, different solvents, and different alkyl halides, are presented.

In this work, the collinear potential energy surface is generated from the three RSs of eq. (2). The transition between these RSs formally represents a two-step mechanism. The first step is an S_N1-type reaction, where the electrophilic agent is generated. This step is referred to as step A. The second step is an S_E2-type reaction, referred to as step B. In general, an S_E2 mechanism is analogous to the S_N2 mechanism in that the new bond is forming as the old one is breaking. In the S_N2 case, however, the incoming group brings a pair of electrons and the orbital that is occupied by the unshared electron pair can overlap only with the central carbon atom while the leaving group takes away its electrons. The process takes place through a backside attack and with inversion of configuration. The situation is quite different in the S_E2-type reaction. It also involves three centers, but only two electrons instead of the four electrons of the S_N2 reaction. Thus, the incoming group may also approach from the front side, because it involves only a vacant orbital. This process takes place with retention of configuration and a cyclic transition state structure.[11] Nevertheless, a solvent with a high nucleophilic character may participate in the process and assist the leaving group. In this case, an open transition state structure with a backside attack and with inversion of configuration would be obtained.[31]

REFERENCE REACTION

Previous *ab initio* calculations at the Hartree–Fock 6-31G(d) level, without the linearity restrictions imposed in the present work, lead to a cyclic transition state structure for the $FCH_3 + CH_4 \rightarrow CH_3CH_3 + HF$ reaction in gas phase.[18] This transition state corresponds to a concerted process, where the heterolytic cleavage, electrophilic attack, and assistance of the forming anion to the leaving proton take place simultaneously. As stated in the Introduction, we restricted ourselves to the study of the potential surface along the collinear path, although the lowest energy transition state may correspond to the cyclic structure in the diagram (see Introduction).

Figure 2 shows the gas-phase *ab initio* potential energy surface for the system in Figure 1. The surface was evaluated at the 6-31G(d) level on the

TABLE VIII.
***Ab Initio* and Experimental Relevant Energy Values for Model Reaction in Gas Phase and in Solution (in kcal/mol).**

Process	*Ab Initio*		Experimental[a]	
	ΔE^{gas}	$\Delta E^{gas} + \Delta\Delta G^{solv}$	ΔE^{gas}	$\Delta E^{gas} + \Delta\Delta G^{solv}$
$I \rightarrow TS_{I\rightarrow II}$	—	111.3		
$I \rightarrow II$	236.4	110.1	257[b]	60.3[c]
$II \rightarrow TS_{II\rightarrow III}$	−4.2	6.91		
$II \rightarrow III$	−36.7	−56.8	−65.5[d]	−73.2[e]
$I \rightarrow III$	199.7	53.3	187.7	−12.9

[a] Obtained from data in Tables I–VII, and taking $D^0_{298}(H—CH_3) = 105.0$ kcal/mol and $D^0_{298}(CH_3—CH_3) = 90.0$ kcal/mol.[39]
[b] $\Delta E^{gas}_{I\rightarrow II} = Diss(F—CH_3) - EA(F^-) + IP(CH_3^+)$.
[c] $\Delta\Delta G^{solv}_{I\rightarrow II} = \Delta G_{solv}(F^-) + \Delta G_{solv}(CH_3^+) - \Delta G_{solv}(CH_3F)$.
[d] $\Delta E^{gas}_{II\rightarrow III} = Diss(H—CH_3) - IP(CH_3^+) + IP(H^+) - Diss(CH_3—CH_3) + PA(H_2O)$.
[e] $\Delta\Delta G^{solv}_{II\rightarrow III} = \Delta G_{solv}(H_3O^+) + \Delta G_{solv}(CH_3—CH_3) - \Delta G_{solv}(CH_3^+) - \Delta G_{solv}(CH_4) - \Delta G_{solv}(H_2O)$.

points of the grid constructed as explained in the Methodology section. Roman numbers (I), (II), and (III) correspond to the three different RSs in eq. (2). We also included the schemes of these RSs and several additional molecules that will be considered in what follows. In Figure 2, *solv* stands for the water molecule in the reference reaction and *cat* stands for the catalyst, which is not included, however, in the calculations that were used to generate Figure 2. From this figure, we obtained the data for the first column in Table VIII. As can be seen from the table, at this level of theory step A is endoergic by approx. 236 kcal/mol, whereas step B occurs without an energy barrier, being exoergic by approx. 37 kcal/mol (with a final endoergicity for the global reaction of about 200 kcal/mol).

Let us consider the effect of the solvent water on the reaction studied in Figure 1. The free energy surface for this reaction in solution was evaluated by CHEMSOL, as explained in the Methodology section, and is shown in Figure 3. Apparently, in contrast to the situation in the gas phase, the heterolytic cleavage of the C—F bond is more favorable than the homolytic one, leading to a stabilization of step A. Nevertheless, given that the process remains very endergonic (about 110 kcal/mol), in agreement with Hammond's principle the transition state is only slightly less stable than the final products (about 2.5 kcal/mol). Now, in contrast to the situation in the gas phase, step B is not barrierless in solution, presenting an energy barrier of 7 kcal/mol. This feature of S_E2-type reactions is also common for S_N2-type reactions, and is due to the fact that the polarity of reactants and products is larger than that of the transition state. The global process for transfer from RS I to RS III is still endergonic by 53 kcal/mol. The experimental value for this global process, as calculated from data in Tables I–VII, is −12.9 kcal/mol. This very large disagreement between CHEMSOL//6-31G(d) calculations and the experimental value is mainly due to the small basis set used in these *ab initio* calculations. That is, this small basis set is not extended enough to capture the behavior of the fluoride anion in the gas phase. Thus, for example, the gas-phase heterolytic

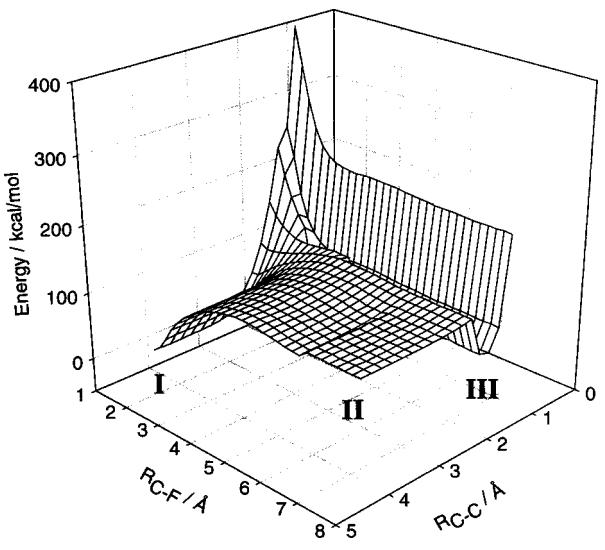

FIGURE 3. *Ab initio* 6-31 G(d) potential energy surface plus free energy of solvation evaluated with CHEMSOL for the reference reaction $FCH_3 + CH_4 + H_2O \rightarrow F^- + CH_3CH_3 + H_3O^+$ in water.

cleavage in the HF molecule is expected to be approximately 364 kcal/mol,[14a] whereas the *ab initio* result for this heterolytic cleavage, at the Hartree–Fock level, is 409 kcal/mol with the 6-31G(d) basis set and 381 kcal/mol with the somewhat more extended 6-311+G(d,p) basis set. (The inclusion of correlation energy does not affect this result much, and we obtained 411 kcal/mol for the heterolytic cleavage in the gas phase at the MP2//6-31G(d) level.[32]) We could, of course, use a more extended basis set but the main aim in the present work is not to develop reliable but expensive *ab initio* surfaces for a single system. Rather, our aim is to develop a reliable EVB approach suitable for being used in general studies of catalysis and, using our strategy, it is quite simple to correct this disagreement between *ab initio* and experimental data by using a proper EVB calibration procedure (*vide infra*).

The next step in our study involved calibrating an EVB surface by requiring it to first reproduce the *ab initio* solution results in Figure 3, and later the experimental results. It is necessary to use *ab initio* calculations for the calibration procedure as experimental data are not available for points along the reaction path. The first parameterization has been carried out by means of a genetic algorithm as explained earlier, and a further correction has been included to reproduce the experimental data. The EVB surface has been fitted to the CHEMSOL//6-31G(d) surface at five points, namely the three points on the surface representing the minimum energies for each RS and the two points with maximum energy connecting them in the proposed stepwise mechanism. The parameters considered were A_{12}, A_{23}, μ_{23} (preliminary GA calculations showed us that taking $\mu_{12} = 0$ is a good approximation and speeds up our finer parameterization) and the three $\alpha^{(i)}$ shifts. In this way, we have considered a constant resonance integral for the S_N1 process and assumed the resonance integral between RS I and RS III to be zero. The fitted parameters are given in Table IX. As can be seen from the table, the value for the A_{23} parameter is apparently very large. This large value mimics, in some way, the existence of other possible RSs in the treatment of step B. The surface obtained in this way was corrected by the energy differences found between the CHEMSOL//6-31G(d) calculations and the experimental values. This further correction was done by changing the $\alpha^{(i)}$ values obtained from the fitting procedure to get the correct asymptotic behavior of our model surface. These $\alpha^{(i)}_{\text{correc,wat}}$ values are also given in Table IX, and the final EVB surface is given in Figure 4. Note that this surface is not completely smooth. This is due to the use of the LD approach to evaluate the solvation energy for the reaction. As explained in the Introduction, not only smoother but also more reliable results could be obtained by higher level EVB/FEP calculations.

TABLE IX.
Parameters for EVB Surface Fitting.[a]

$i-j$	A_{ij}	μ_{ij}	i	$\alpha^{(i)}$	$\alpha^{(i)}_{\text{correc,wat}}$	$\alpha^{(i)}_{\text{correc,HF}}$
I–II	9.3	0.0	I	−26.8	−26.8	−26.8
I–III	0.0	0.0	II	289.1	209.2	183.3
II–III	1136.0	0.53	III	199.4	139.0	159.6

[a] $\alpha^{(i)}_{\text{correc,wat}}$ and $\alpha^{(i)}_{\text{correc,HF}}$ values are the base where the reaction-specific $\Delta\alpha^{(i)}$ is to simulate the different reactions in this work (see text).

In order to illustrate the main features of the EVB surface and to examine its validity we considered sections of this surface along the A and B pathways (by taking the cross-sections corresponding to the fixed distances $R_{C\text{—}C} = 4.08$ Å and $R_{F\text{—}C} = 7.37$ Å, respectively). A wider exploration of the surfaces, extending it to the asymptotic regions, would be preferable in a more complete study, but again, to illustrate the method we can assume that our surfaces explore enough of those asymptotic regions by using this limited grid. These sections and the corresponding experimental values are presented in Figure 5a and b for step A and step B, respectively. Step A, as an S_N1-type process, is expected to

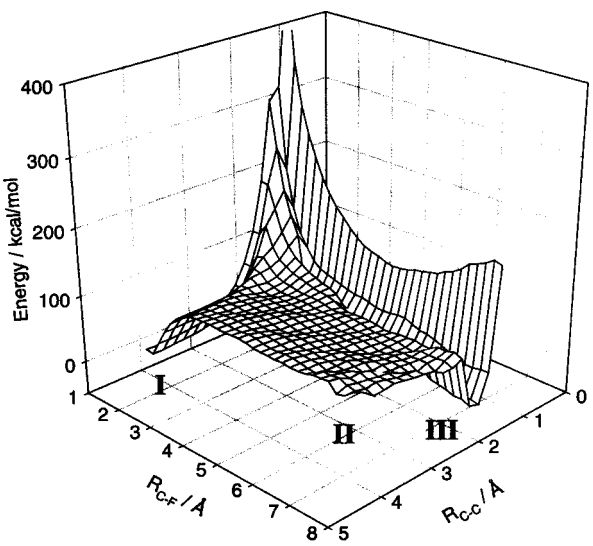

FIGURE 4. Global solvation free-energy EVB surface for the hypothetical reference reaction $FCH_3 + CH_4 + H_2O \rightarrow F^- + CH_3CH_3 + H_3O^+$ in water.

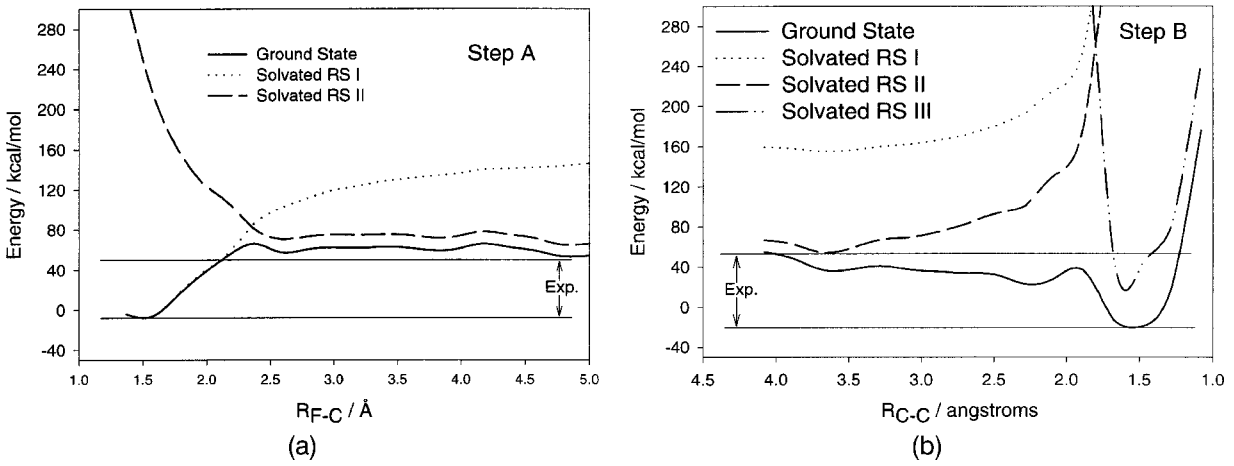

FIGURE 5. (a) Free-energy EVB profile for the S_N1-type process (step A) in the hypotethical reference reaction $FCH_3 + CH_4 + H_2O \rightarrow F^- + CH_3^+ + CH_4 + H_2O$ in water. The experimental value for the global process is 60.3 kcal/mol (see Table VIII). (b) Free-energy EVB profile for the S_E2-type process (step B) $F^- + CH_3^+ + CH_4 + H_2O \rightarrow F^- + CH_3CH_3 + H_3O^+$ in the reference reaction. The experimental value for the global process is −73.2 kcal/mol (see Table VIII).

present major contributions from the covalent RS in the reactants region and from the ionic diabatic surface in the products region. The third RS presents a much higher energy and does not contribute to the ground-state energy. The reverse process of association between F^- and CH_3^+ presents a free energy of activation of about 10 kcal/mol. As for step B, we can see how use of the $\alpha^{(i)}_{\text{correc,wat}}$ values masks the possible existence of the free energy barrier. In this case, the main contributions to the ground-state free energy surface come from the second RS at the reactants region and from the third one at the products region. Note that the resonance integral, H_{23}, is very large, causing about a 120 kcal/mol difference between the diabatic and the adiabatic surfaces at the transition state. A further refinement of the present potential energy surface could come from the use of more RSs, allowing the EVB procedure to fit the global surface more adequately.

DUAL ROLE OF SOLVENT AS REACTANT AND AS ENVIRONMENT

Before moving to more general alkylation reactions we consider the general role of the solvent. This is done by considering the change of the solvent from water to nitromethane. Here again, we do not yet deal with a real Friedel–Crafts-type reaction, but we are merely trying to demonstrate the effectiveness of the EVB method in modeling changes in both chemistry and solvation. That is, in the case of nitromethane, we must consider two factors: (i) the change of the proton acceptor from H_2O to CH_3NO_2 in reaction (1), which can be written as:

$$CH_3F + CH_4 + CH_3NO_2 \rightarrow F^- + CH_3CH_3 + CH_3NO_2{-}H^+ \quad (10)$$

and (ii) the change of the solvent from water to nitromethane. The examination of their effect could be done in principle by repeating the *ab initio* calibration of the model reaction while replacing H_2O by CH_3NO_2. However, in the EVB formulation, we can capture most of the effect of changing H_2O to CH_3NO_2 by changing $\alpha^{(3)}$ to account for the corresponding change in proton affinity. This change is $\Delta\alpha^{(3)} = 52.9$ kcal/mol, as calculated from Scheme 1 using data from Table V. Adding this $\Delta\alpha^{(3)}$ to $\alpha^{(3)}_{\text{correc,wat}}$ provides a way of simulating the change of the proton acceptor without reevaluating the relevant potential surface by *ab initio* calculations.

The second factor, the effect of the solvent polarity, is obtained simply by scaling the LD solvation energy using the Onsager relationship:

$$\Delta G_{sol}(\varepsilon') = \Delta G_{sol}(\varepsilon)\frac{2\varepsilon' - 2}{2\varepsilon + 1} \quad (11)$$

assuming that the cavity radius remains the same. The dielectric constant for water is taken to be 80.0 and for nitromethane is 34.3.[47] Note that, although the use of the Onsager cavity model is very qualitative, the scaling of reliable solvation energies by the Onsager dielectric factor [i.e., using eq. (11)] gives quantitative results. Using the $\Delta\alpha^{(3)}$ shift and eq. (11), we find that step A in nitromethane is less favorable than the same process in water by

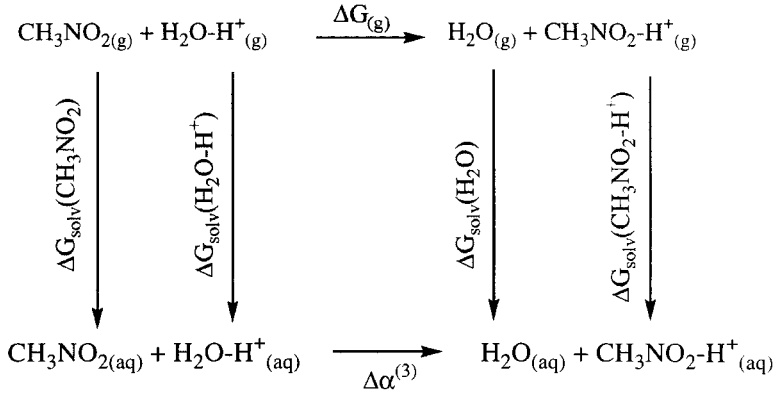

$$\Delta G_{(g)} = PA(CH_3NO_2) - PA(H_2O)$$

$$\Delta\alpha^{(3)} = \Delta G_{solv}(H_2O) + \Delta G_{solv}(CH_3NO_2\text{-}H^+) - \Delta G_{solv}(CH_3NO_2) - \Delta G_{solv}(H_2O\text{-}H^+) + \Delta G_{(g)}$$

SCHEME 1.

about 40 kcal/mol. Step B is even more affected, as can be seen from Figure 6 (note that this figure involves the global reaction through step A and step B). The main factor is the different solvation of the protonated proton acceptor in water and in nitromethane. Although the proton affinity of nitromethane is 13.5 kcal/mol higher than the proton affinity of water, the final solvation is dramatically reversed, because the solvation of the hydronium ion is clearly higher (−102 kcal/mol) than the solvation of the protonated nitromethane (−60 kcal/mol). Thus, step B in nitromethane is found to be endergonic, making the overall reaction unaccessible at room temperature. One way to make this reaction accessible at room temperature would be the addition of a Lewis acid catalyst like BF_3 or SbF_5. The role of these catalysts, as is explained next, is mainly to assist the emerging fluoride anion and form a very stable cat-F^- compound. However, the nitromethane will bind the catalyst and make it unavailable for the reaction. Thus, we must also consider the "chemistry" between the solvent and the catalyst. In this sense, a much clearer picture of the role of BF_3 and SbF_5 emerges via HF study.

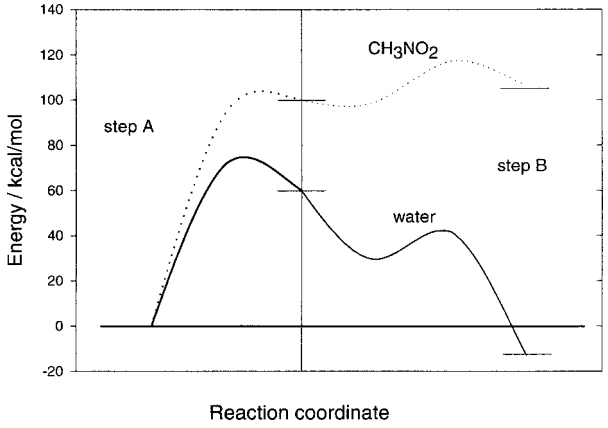

FIGURE 6. The role of the solvent by schematic demonstration of the free-energy profiles for the stepwise mechanism for reactions in the following solvents: water (solid line, model reaction); and nitromethane (dotted line).

REACTION IN HF

As stated in the beginning of the Methodology section, the reaction described by eq. (1) does not occur in water. Similarly, reaction (10) does not occur in nitromethane and cannot be catalyzed in this solvent because of the problem mentioned at the end of the last section. However, when HF is the solvent, we have the reaction:

$$CH_3F + CH_4 + 2HF \rightarrow HF_2^- + CH_3CH_3 + H_2F^+ \quad (12)$$

where the HF molecule acts both as a proton acceptor and as a stabilizer for the F^- ion. As shown in the previous section we can take the surface for the reaction of eq. (1) in solution (Fig. 3) and change it to the surface of eq. (12). This is done by changing the $\alpha^{(i)}$ values for the global EVB. The $\alpha^{(2)}$ value is changed following Scheme 2 ($\Delta\alpha^{(2)} = -25.9$ kcal/mol), and the $\alpha^{(3)}$ value is changed following Scheme 3 ($\Delta\alpha^{(3)} = 20.6$ kcal/mol). The $\alpha^{(i)}$ values obtained

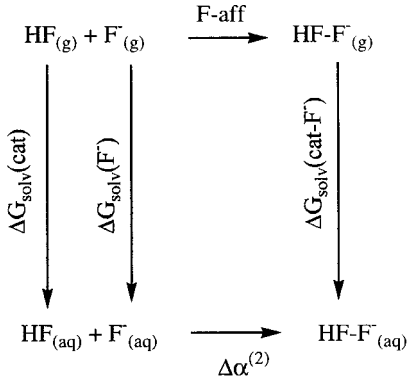

$$\Delta\alpha^{(2)} = \Delta G_{solv}(HF\text{-}F^-) - \Delta G_{solv}(HF) - \Delta G_{solv}(F^-) + \text{F-aff}$$

SCHEME 2.

in this way are given in the last column of Table IX. These parameters are referred to as $\alpha^{(i)}_{correc,HF}$ to distinguish them from the previous water-based $\alpha^{(i)}_{correc,wat}$ values. Also, as was done in the previous subsection, we simulate the change of the solvent from water to HF by simply applying the Onsager relationship shown in eq. (11), taking $\varepsilon_{HF} = 84$ at 273 K.[39]

The calculated potential surface for reaction (12) in HF is shown in Figure 7. As is apparent from the figure, the effect of changing the solvent from the hypothetical H_2O, used in from the previous model calculations, to the more realistic HF is dramatic. In step A, the loss of approximately 20 kcal/mol of solvation energy in going from the fluoride anion to the HF_2^- anion is clearly overcompensated by the strong

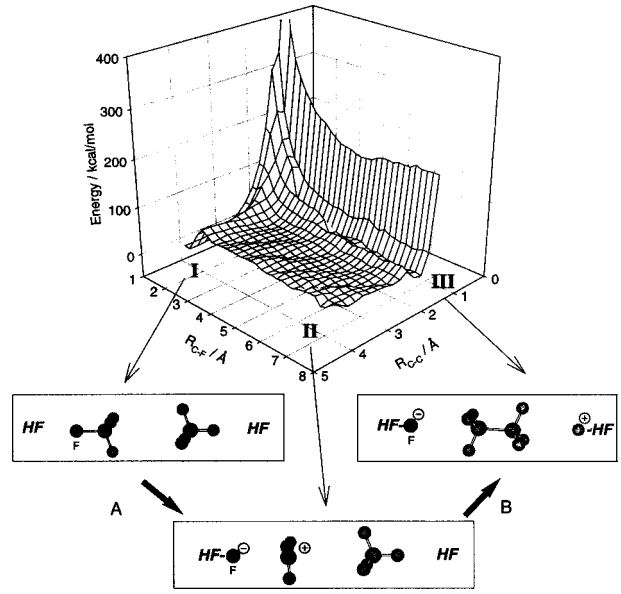

FIGURE 7. Global EVB free-energy surface for the reaction $HF + FCH_3 + CH_4 + HF \rightarrow HF_2^- + CH_3CH_3 + H_2F^+$ modeled using the data from the reference reaction and the $\alpha^{(i)}_{correc,HF}$ from Table IX. The three resonance structures used to construct the global surface are indicated.

fluoride affinity of HF (−51.5 kcal/mol), being the driving force for this process. On the contrary, step B is not favored due to the lower proton affinity of HF with respect to H_2O, but the global process is still controlled by step A. The addition of better fluoride acceptors, as noted in what follows, is the driving force for the whole reaction.

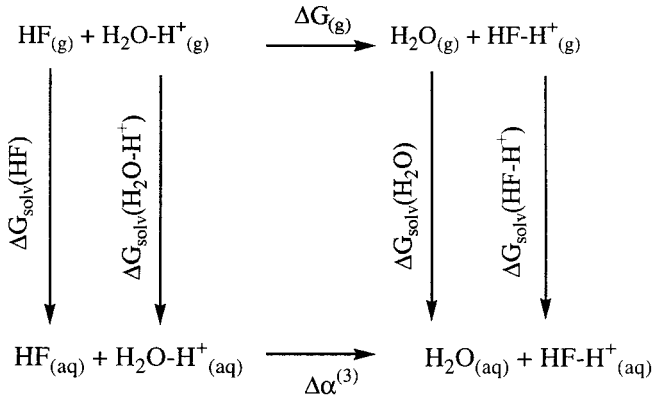

$$\Delta G_{(g)} = PA(HF) - PA(H_2O)$$

$$\Delta\alpha^{(3)} = \Delta G_{solv}(H_2O) + \Delta G_{solv}(HF\text{-}H^+) - \Delta G_{solv}(HF) - \Delta G_{solv}(H_2O\text{-}H^+) + \Delta G_{(g)}$$

SCHEME 3.

EVB/SHIFTS ANALYSIS OF CATALYTIC EFFECTS

Role of Catalyst. Similar to the method we used to include the changes in the solvent by shifting the diabatic surfaces for the significant RSs in the reference reaction, we can include the effects of other factors by similar EVB/shifts. The EVB/shifts introduce the effects of the different factors involved in the global process (e.g., catalyst or substituent)[14, 33] by shifting the corresponding diabatic potential energy surfaces in the gas phase [the $\alpha^{(i)}$ in eq. (3)]. The analysis presented involves modifications of the HF-solvated reaction. Thus, the free energy changes produced by the different substitutions in what follows are all based on the $\alpha^{(i)}_{\text{correc,HF}}$ values and all the solvation energies for the final EVB surfaces calculated by making use of the Onsager relationship in eq. (11). We first consider the BF_3 catalyst. This molecule stabilizes F^- by converting it to BF_4^-. For example, in the RSs II and III:

$$F^- + CH_3^+ + CH_4 + HF + BF_3 \rightarrow BF_4^- + CH_3^+ + CH_4 + HF \quad (13)$$

$$F^- + CH_3{-}CH_3 + H_2F^+ + BF_3 \rightarrow BF_4^- + CH_3{-}CH_3 + H_2F^+ \quad (14)$$

In principle, we could represent this effect by adding additional RSs that represent the products of the reactions in eqs. (13) and (14). However, because we are not interested in the surface for the F^- transfer to BF_3 (this is not the rate-determining step), we can simply introduce this effect of BF_3 by modifying the gas-phase shifts of state II and state III. In other words, we can introduce the effect of a catalyst within the EVB philosophy by changing the diagonal energies of the relevant states. Globally, the shift of the diagonal elements of the Hamiltonian in states II and III is given by Scheme 4.

Other catalysts can be considered in the same way and we show the results for BF_3 and SbF_5 (a very strong catalyst commonly used in Friedel–Crafts reactions).[34] With data taken from Tables VI and VII, we obtain values for $\Delta\alpha^{(2)}$ of −11.5 and −34.4 kcal/mol for the BF_3 and SbF_5 EVB surfaces, respectively. The catalyst changes only the profile for step A, leaving the profile for step B unchanged. Thus, $\Delta\alpha^{(2)}$ is equal to $\Delta\alpha^{(3)}$, because step B does not involve any contribution from the catalyst. The global surface obtained for BF_3 is shown in Figure 8. The figure shows that the shape of this global surface resembles that of the HF-catalyzed reaction (where an HF molecule assisted the emerging F^-), but in this case RSs II and III are stabilized with respect to the HF-catalyzed result. This can be seen more clearly in Figure 9, where, as was done in Figure 6, we show schematically the results for the global process. Clearly, it is the catalyst molecule that assists the emerging fluoride anion by increasing the driving force for step A in just the same way as the solvent molecule does for the proton in step B. At any rate, the overall result (which is expected to hold for the actual transition state) is that the catalyst decreases dramatically the activation free energy of the process. The calculated free-energy barrier obtained from the global surface for the concerted processes are 46.0, 42.0, and 31.0 kcal/mol for the uncatalyzed, BF_3-catalyzed, and SbF_5-catalyzed reactions, respectively. This EVB consideration appears to provide a useful insight into the role of the Lewis-acid catalyst in Friedel–Crafts reactions.

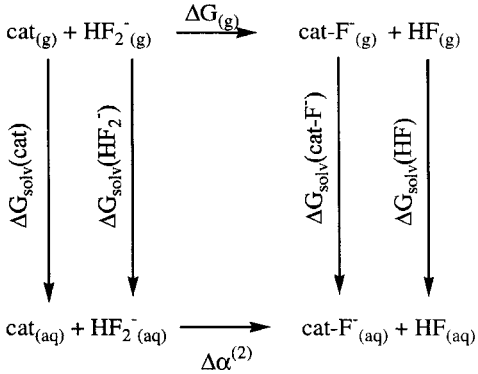

$$\Delta G_{(g)} = \text{F-aff(cat)} - \text{F-aff(HF)}$$

$$\Delta\alpha^{(2)} = \Delta\alpha^{(3)} = \Delta G_{solv}(\text{cat-F}^-) + \Delta G_{solv}(\text{HF}) - \Delta G_{solv}(\text{cat}) - \Delta G_{solv}(\text{HF}_2^-) + \Delta G_{(g)}$$

SCHEME 4.

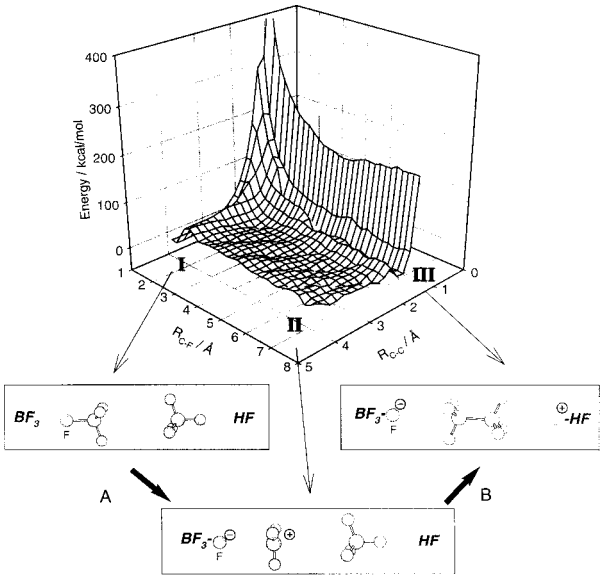

FIGURE 8. Global EVB free-energy surface for the reaction $BF_3 + FCH_3 + CH_4 + HF \rightarrow BF_4^- + CH_3CH_3 + H_2F^+$ modeled using the data from the reference reaction and $\alpha^{(i)}_{correc,HF}$ from Table IX and the $\Delta\alpha^{(i)}$ indicated in the text. The three resonance structures used to construct the global surface are shown.

A more relevant result can be obtained by examining the shift of the free energy of the actual transition state, which may reside on the concerted path or the three-center bond transition state. This is, however, beyond the scope of the present work.

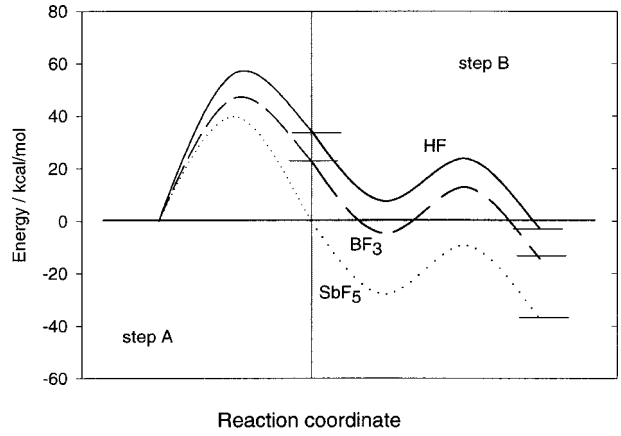

FIGURE 9. The effect of catalysts by schematic plot of the free-energy profile in HF solution for the stepwise mechanism of the uncatalyzed (solid line), BF_3-catalyzed (dashed line), and SbF_5-catalyzed (dotted line) reactions.

Role of Substituents. The EVB/shifts approach also provides an extremely convenient way of exploring the effect of substituents on chemical reactions. In the present case, we consider the reactions:

$$HF + FR + CH_4 + HF \rightarrow HF_2^- + R^+ + CH_4 + HF \quad (15)$$

$$HF_2^- + R^+ + CH_4 + HF \rightarrow HF_2^- + R{-}CH_3 + H_2F^+ \quad (16)$$

and the trend in going from primary to secondary and tertiary alkyl halides (R = methyl, ethyl, *i*-propyl, and *t*-butyl). Here, we change the gas-phase

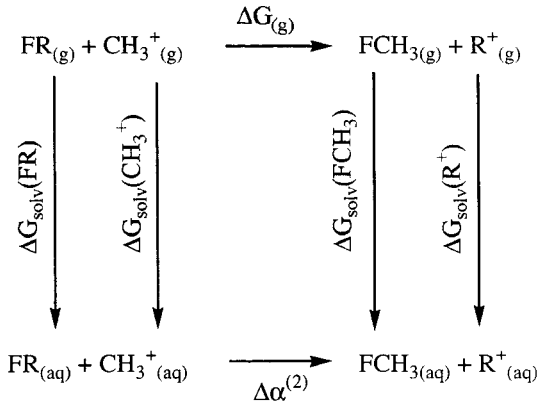

$$\Delta G_{(g)} = [Diss(F\text{-}R) + IP(R)] - [Diss(F\text{-}C) + IP(CH_3)]$$

$$\Delta\alpha^{(2)} = \Delta G_{solv}(FCH_3) + \Delta G_{solv}(R^+) - \Delta G_{solv}(FR) - \Delta G_{solv}(CH_3^+) + \Delta G_{(g)}$$

SCHEME 5.

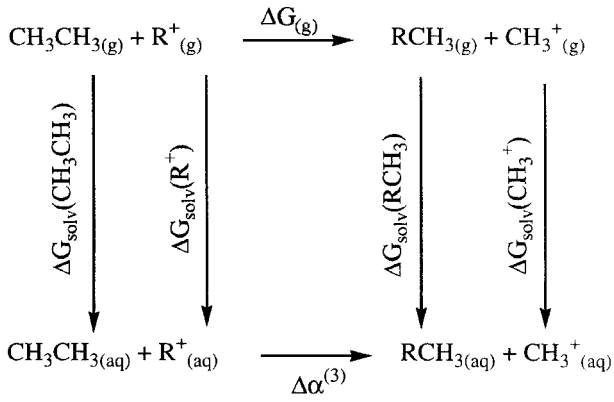

$$\Delta G_{(g)} = [\mathrm{Diss(C\text{-}C)} + \mathrm{IP}(CH_3)] - [\mathrm{Diss(R\text{-}C)} + \mathrm{IP(R)}]$$

$$\Delta\alpha^{(3)} = \Delta G_{solv}(RCH_3) + \Delta G_{solv}(CH_3^+) - \Delta G_{solv}(CH_3CH_3) - \Delta G_{solv}(R^+) + \Delta G_{(g)}$$

SCHEME 6.

shift in the S_N1 reaction by $\Delta\alpha^{(2)}$, according to Scheme 5 and the gas-phase shift in the S_E2 process, $\Delta\alpha^{(3)}$, following Scheme 6.

Using data from Tables I, II, and III, we obtain (in kcal/mol) $\Delta\alpha^{(2)}_{\text{ethyl}} = -6.5$, $\Delta\alpha^{(2)}_{i\text{-propyl}} = -24.3$, and $\Delta\alpha^{(2)}_{t\text{-butyl}} = -26.1$, for step A, and $\Delta\alpha^{(3)}_{\text{ethyl}} = -1.1$, $\Delta\alpha^{(3)}_{i\text{-propyl}} = -2.6$, and $\Delta\alpha^{(3)}_{t\text{-butyl}} = -0.6$, for step B (recall that $\Delta\alpha^{(3)}$ values include $\Delta\alpha^{(2)}$). After recalculating the EVB energy surface in solution we reiterate the fact that the alkylation rate constant increases upon going from primary to tertiary halides.[2–4] Figure 10 schematically presents the change in activation free energy for methyl, ethyl, *i*-propyl, and *t*-butyl fluorides. The change in the driving force for step A comes mainly from the different ionization potential of the several alkyl species, the different solvation of these species, and to a minor degree from the different dissociation energy of the carbon–fluorine bond. The variation in step B arises from changes in the solvation energies and heats of formation of the alkyl cations and the adduct products in which a new carbon–carbon bond is formed. As a final result of the calculated driving forces for both steps, one can see in Figure 10 that the free energy barrier decreases going from the methyl to the *t*-butyl fluorides in the series. The calculated free-energy barrier obtained from the global surface for the concerted processes are 46.0, 44.0, 41.0, and 40.0 kcal/mol for the methyl, ethyl, *i*-propyl, and *t*-butyl reactions, respectively.

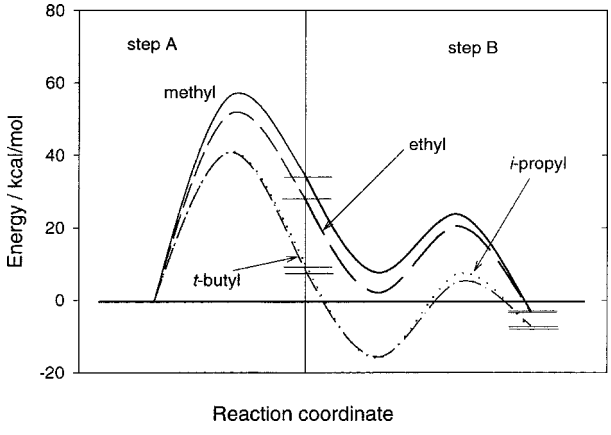

FIGURE 10. The effect of alkylation agents by schematic plot of the free-energy profile in HF solution for the stepwise mechanism of reactions with several alkyl substituents [*R* in eqs. (15) and (16)]: methyl (solid line); ethyl (dashed line); *i*-propyl (dotted line); and *t*-butyl (dashed-dotted line).

Conclusions

In this work we have demonstrated the use of a simple version of the EVB method that represents the solvent by the LD model in qualitative studies of the role of different factors in complex reactions. To illustrate this methodology, we applied it to collinear configurations of Friedel–Crafts-type alkylation reactions. Concretely, we have studied the effect produced on the free-energy surface when changing the solvent, the catalyst, and the alkylation agent.

The EVB methodology in this simple approach appears to be quite useful in providing a good estimate for the shape of the free-energy surface for the reactions considered, giving the proper balance between computational cost and chemical predictivity, which is the goal of the computational chemist.

The present study was restricted to polar solvents with a high nucleophilic character. Otherwise, a cyclic transition state may be expected. The effect of the solvent on a Friedel–Crafts model reaction has been studied previously using a continuum model,[36] but it seems to us that the simple EVB/LD model used in the present work captures more precisely the physics of the solvation in this reaction and allows one to model the actual catalysis.

Also in this investigation we have parameterized the potential energy surface for a Friedel–Crafts-type reference reaction, which is, by itself, only a hypothetical reaction, using *ab initio* calculations and experimental data. Beginning with this surface we have simulated a series of Friedel–Crafts-type alkylation reactions to investigate the role of different elements in this general type of reaction. In considering the stepwise mechanism, we have found that very polar solvents are required to stabilize the products of step A, which is, in turn, the rate-limiting step of the overall reaction. After considering the hypothetical effect of different solvents we moved to the more realistic case where HF serves as a solvent. In this case, the HF molecule plays a double chemical role accepting the fluoride anion emerging from the S_N1 process (acting in this way as a Lewis acid catalyst) and accepting the proton generated in step B. We have examined the trend going from the uncatalyzed reaction through the $HF/BF_3/SbF_5$ series. As expected, we have found that step A becomes progressively more favored. Finally, the role of the alkylation agent employed in the Friedel–Crafts reaction has been examined and found to follow the experimental trend whereby the reaction is favored upon going from primary to tertiary alkyl compounds.

The present approach clearly can be improved by exploring the noncollinear parts of Friedel–Crafts-type reactions. In particular, one could examine the paths that lead to the three-center bond transition state. This can be done quite effectively by adding more EVB RSs. However, a study of the complete potential energy surface may make our discussion more complicated and shift the focus from the main objective of this work, which is illustration of the effectiveness of the EVB method as a general tool for modeling solvation and catalytic effects in very complex reactions. It is also quite likely that the energy changes of the lowest transition state are correlated with the energy changes of the collinear transition state. The methodology presented herein can be applied to a wide range of complex problems, where the EVB/shifts for generating the different final surfaces can easily be calculated from thermodynamic data.

Acknowledgments

J. V. acknowledges Berta Alsina and Arnau Villà for personal support. We would also like to thank Profs. George A. Olah and G. K. Surya Prakash for insightful comments.

References

1. (a) Friedel, C.; Crafts, J. M. Comput Rend 1877, 84, 1450; (b) Friedel, C.; Crafts, J. M. Comput Rend 1877, 85, 74.
2. Olah, G. A. In: Olah, G. A., Ed. Friedel–Crafts and Related Reactions, Vol. I; Wiley: New York, 1963; p. 25.
3. Olah, G. A.; Pavlath, A.; Olah, J. J Chem Soc 1957, 2174.
4. Drahowzal, F. A. In: Olah, G. A., Ed., Friedel–Crafts and Related Reactions, Vol. II; Wiley: New York, 1964; p. 417.
5. Olah, G. A. In: Olah, G. A., Ed. Friedel–Crafts and Related Reactions, Vol. I; Wiley: New York, 1963; p. 201.
6. Bazz, M.; Gutmann, V. In: Olah, G. A., Ed., Friedel–Crafts and Related Reactions, Vol. I; Wiley: New York, 1963; p. 367.
7. (a) Jenny, R. Comput Rend 1958, 246, 3477; (b) Jenny, R. Comput Rend 1959, 248, 3555; (c) Jenny, R. Comput Rend 1960, 250, 1659.
8. (a) Nakana, R.; Oyana, T. J Phys Chem 1966, 70, 1146; (b) Nelson, H. M. J Phys Chem 1962, 66, 1380; (c) Olah, G. A.; DeMember, R. H.; Schlosberg, R. H. J Am Chem Soc 1970, 92, 2562; (d) Olah, G. A.; DeMember, J. H.; Schlosberg, R. H.; Halpem, Y. J Am Chem Soc 1972, 94, 156; (e) Olah, G. A.; Meyer, M. M. In: Olah, G. A., Ed., Friedel–Crafts and Related Reactions, Vol. I; Wiley: New York, 1963; p. 623.
9. Olah, G. A.; Prakash, G. K. S.; Williams, R. E.; Field, L. D.; Wade, K. In: Hydrocarbon Chemistry; Wiley: New York, 1987.
10. (a) Brown, H. C.; Grayson, M. J Am Chem Soc 1953, 75, 6285; (b) Jungk, H.; Smoot, C. R.; Brown, H. C. J Am Chem Soc 1956, 78, 2185; (c) Brown, H. C.; Belta, B. A. J Am Chem Soc 1959, 81, 3520.
11. (a) Olah, G. A.; Klopman, G.; Schosberg, H. J Am Chem Soc 1969, 91, 3261; (b) Olah, G. A. Angew Chem Int Ed 1973, 12, 173.
12. (a) Epiotis, N. D.; Larson, J. R.; Eaton, H. In: Unified Valence Bond Theory of Electronic Structure; Springer: Heidelberg, 1982; (b) Shaik, S. S.; Pross, A. J Am Chem Soc 1982, 104, 2708; (c) Pross, A.; Shaik, S. S. Acc Chem Res 1983, 16, 363; (d) Shaik, S. S. Prog Phys Org Chem 1985, 15, 197.
13. (a) Bernardi, F.; Robb, M. A. Adv Chem Phys 1987, 67, 155; (b) Bernardi, F.; McDowall, J. J. W.; Robb, M. A. J Comput Chem 1987, 8, 296; (c) Bernardi, F.; Robb, M. A. J Am Chem

Soc 1984, 106, 54; (d) Bernardi, F.; Olivucci, M.; Robb, M. A. Acc Chem Rev 1990, 23, 405.

14. (a) Warshel, A. In: Computer Modeling of Chemical Reactions in Enzymes and in Solutions; Wiley: New York, 1991; (b) Warshel, A.; Weiss, R. M. J Am Chem Soc 1980, 102, 6218; (c) Warshel, A.; Sussman, F.; Hwang, J. K. J Mol Biol 1988, 201, 139; (d) Hwang, J. K.; King, G.; Creighton, S.; Warshel, A. J Am Chem Soc 1988, 110, 5297; (e) Åqvist, J.; Warshel, A. Biochemistry 1988, 28, 4680; (f) Åqvist, J.; Warshel, A. Chem Rev 1993, 93, 2523; (g) Lee, F. S.; Chu, Z. T.; Warshel, A. J Comput Chem 1993, 14, 161.
15. (a) Kim, H. J.; Hynes, J. T. Int J Quantum Chem Quantum Chem Symp 1990, 24, 821; (b) Kim, H. J.; Hynes, J. T. J Am Chem Soc 1992, 114, 10508; (c) Kim, H. J.; Hynes, J. T. J Am Chem Soc 1992, 114, 10528; (d) Chang, Y.-T.; Miller, W. H. J Phys Chem 1990, 94, 5884; (e) Chang, Y.-T.; Minichino, C.; Miller, W. H. J Chem Phys 1992, 96, 4341; (f) Bala, P.; Grochowski, P.; Lesyng, B.; McCammon, J. A. In: Bicout, D.; Field, M., Eds., Quantum Mechanical Simulation Methods for Studying Biological Systems; Springer: Berlin, 1995; p. 119; (g) Grochowski, P.; Lesyng, B.; Bala, P.; McCammon, J. A. Int J Quantum Chem 1996, 60, 1143; (h) Bala, P.; Grochowski, P.; Lesyng, B.; McCammon, J. A. J Phys Chem 1996, 100, 2535; (i) Lobaugh, J.; Voth, G. A. J Chem Phys 1994, 100, 3039; (j) Neria, E.; Karplus, M. 1997, 267, 23; (k) Vuilleumier, R.; Borgis, D. Chem Phys Lett 1998, 284, 71; (l) Schmitt, U. W.; Voth, G. A. J Phys Chem 1998, 102, 5547; (m) Kim, Y.; Corchado, J. C.; Villà, J.; Xing, J.; Truhlar, D. G. J Chem Phys 2000, 112, 2718.
16. Ref. 15g adopted the EVB approach without any change, but then it was argued[15h] that a new microscopic model (called AVB) had been developed. This argument was based on the assertion that the EVB model is calibrated on macroscopic thermodynamic data while the so-called AVB approach is calibrated on *ab initio* gas-phase results. This argument reflects a very problematic perspective. First, the EVB model provides fully microscopic all-atom molecular surfaces that are always calibrated on the most reliable information available at the given time. This, of course, includes *ab initio* results when these results are considered to be sufficiently reliable (e.g., refs. 14d, 15d, and 15i). Second, the argument that calibration of a microscopic model using macroscopic properties makes the model macroscopic is simply misleading. As is now obvious to almost all workers in the field one of the best ways of calibrating microscopic models is the use of these models in simulations of average properties (e.g., solvation free energies) and then using the agreement between the calculated and observed properties in refining the microscopic level. This is, for example, the approach used in refining popular water models and many force fields. Finally, as a note of caution, even now, with very powerful *ab initio* approaches, it is important to verify the calculated results using experimental information about the given reaction in solution. This is demonstrated in the present work and not doing so will lead to incorrect results in calculations of complex systems such as enzymatic reactions.
17. Wesolowski, T.; Warshel, A. J Phys Chem 1994, 98, 5183.
18. Branchadell, V.; Oliva, A.; Bertrán, J. J Chem Soc Perkin Trans II 1989, 1091.
19. Frisch, M. J.; Trucks, G. W.; Schlegel, H. B.; Gill, P. M. W.; Johnson, B. G.; Robb, M. A.; Cheeseman, J. R.; Keith, T. A.; Petersson, G. A.; Montgomery, J. A.; Raghavachari, K.; Al-Laham, M. A.; Zakrzewski, V. G.; Ortiz, J. V.; Foresman, J. B.; Ciolowski, J.; Stefanov, B. B.; Nanayakkara, A.; Challacombe, M.; Peng, C. Y.; Ayala, P. Y.; Chen, W.; Wong, M. W.; Andres, J. L.; Replogle, E. S.; Gomperts, R.; Martin, R. L.; Fox, D. J.; Binkley, J. S.; Defrees, D. J.; Baker, J.; Stewart, J. P.; Head-Gordon, M.; Gonzalez, C.; Pople, J. A. GAUSSIAN-94; Gaussian: Pittsburgh, PA, 1995.
20. Florián, J.; Warshel, A. J Phys Chem 1997, 101, 5583.
21. (a) Florián, J.; Warshel, A. CHEMSOL, version 1.12; University of Southern California: Los Angeles, 1997; (b) Program CHEMSOL can be downloaded from the anonymous ftp server usc.edu, directory /pub/warshel/cs.
22. Miertus, S.; Scrocco, E.; Tomasi, J. J Chem Phys 1981, 55, 117.
23. Kong, Y. S.; Warshel, A. J Am Chem Soc 1995, 117, 6234.
24. Muller, R. P.; Warshel, A. J Phys Chem 1995, 99, 17516.
25. (a) Chandrasekhar, J.; Smith, S. F.; Jorgensen, W. L. J Am Chem Soc 1985, 107, 154; (b) Chandrasekhar, J.; Jorgensen, W. L. J Am Chem Soc 1985, 107, 2974.
26. Villà, J.; Warshel, A. SIMPLEVB, University of Southern California: Los Angeles, CA, 1999.
27. (a) Goldberg, D. E. In: Genetic Algorithms in Search, Optimization & Machine Learning; Addison-Wesley: Reading, MA, 1989; (b) Carroll, D. L. GA, version 1.6.4, University of Illinois at Urbana-Champaign: Urbana, IL, 1997.
28. (a) Villà, J.; González-Lafont, A.; Lluch, J. M.; Truhlar, D. G. J Am Chem Soc 1998, 120, 5559; (b) Villà, J.; Corchado, J. C.; González-Lafont, A.; Lluch, J. M.; Truhlar, D. G. J Am Chem Soc 1998, 120, 12141; (c) Villà, J.; Corchado, J. C.; González-Lafont, A.; Lluch, J. M.; Truhlar, D. G. J Phys Chem A 1999, 103, 5061.
29. Hay, P. J.; Wadt, W. R. J Chem Phys 1985, 82, 299.
30. (a) Hwang, J.-K.; Warshel, A. J Am Chem Soc 1987, 109, 715; (b) Lee, F. S.; Chu, Z. T.; Bolger, M. B.; Warshel, A. Prot Eng 1992, 5, 215.
31. Abraham, M. H. In: Bamford, C. H.; Tipper, C. F. H., Eds., Comprehensive Chemical Kinetics, Vol. 12; Elsevier: Amsterdam, 1973.
32. (a) Krishnan, R.; Binkley, J. S.; Seeger, R.; Pople, J. A. J Chem Phys 1980, 72, 650; (b) Møller, C.; Plesset, M. S. Phys Rev 1934, 46, 618.
33. Warshel, A.; Hwang, J. K.; Åqvist, J. Faraday Discuss 1992, 93, 225.
34. (a) Yakobson, G. G.; Furin, G. G. Synthesis 1980, 345, and references therein; (b) DeHaan, F. P.; Delker, G. L.; Covey, W. D.; Ahn, J.; Anisman, M. S.; Brehm, E. C.; Chang, J.; Chicz, R. M.; Cowan, R. L.; Ferrara, D. M.; Fong, C. H.; Harper, J. D.; Irani, C. D.; Kim, J. Y.; Meinhold, R. W.; Miller, K. D.; Roberts, M. P.; Stoler, E. M.; Suh, Y. J.; Tang, M.; Williams, E. C. J Am Chem Soc 1984, 106, 7038.
35. Kong, Y. S.; Warshel, A. J Am Chem Soc 1995, 117, 6234.
36. Tuñón, I.; Silla, E.; Bertrán, J. J Chem Soc Faraday Trans 1994, 90, 1757.
37. Dean, J. A. Lange's Handbook of Chemistry; McGraw-Hill: New York, 1992.
38. Pearson, R. G. J Am Chem Soc 1986, 108, 6109.
39. Lide, D. R., Ed. Handbook of Chemistry and Physics, 77th ed.; CRC Press: Boca Raton, FL, 1996.
40. Benson, S. W. In: Thermochemical Kinetics; Wiley: New York, 1976.
41. Frenkel, M.; Marsh, K. N.; Wilhoit, R. C.; Kabo, G. J.; Roganov, G. N. In: Thermodynamic of Organics Com-

pounds in the Gas State, Vol. I, TRC Data Series; Thermodynamic Research Center: College Station, TX, 1994.

42. Ben-Naim, A. In: Solvation Thermodynamics; Plenum Press: New York, 1987.
43. Alberty, R. A.; Gehrig, C. A. J Chem Phys Ref Data 1984, 13, 1173.
44. Alberty, R. A. J Chem Phys Ref Data 1985, 14, 177.
45. Lias, S. G.; Liebman, J. F.; Levin, R. D. J Phys Chem Ref Data 1984, 13, 695.
46. Kriemler, P.; Buttrill, S. E., Jr. J Am Chem Soc 1973, 95, 1365.
47. Chelkowski, A. In: Dielectric Physics; Elsevier: Amsterdam, 1980.
48. Meller, A. In: Gmelin Handbook of Inorganic Chemistry, Boron Compounds, Vol. 3, 3rd supplement; Springer: New York, 1988.